






# Flow Z-pinch plasma production on the FuZE experiment

Cite as: Phys. Plasmas **27**, 112503 (2020); <https://doi.org/10.1063/5.0020481>

Submitted: 01 July 2020 . Accepted: 24 September 2020 . Published Online: 03 November 2020

 A. D. Stepanov,  U. Shumlak,  H. S. McLean, B. A. Nelson,  E. L. Claveau,  E. G. Forbes, T. R. Weber, and  Y. Zhang

## COLLECTIONS

Paper published as part of the special topic on [Papers from the 61st Annual Meeting of the APS Division of Plasma Physics DPP61](#)



View Online



Export Citation



CrossMark

## ARTICLES YOU MAY BE INTERESTED IN

### [Z-pinch fusion](#)

Journal of Applied Physics **127**, 200901 (2020); <https://doi.org/10.1063/5.0004228>

### [Plasma exhaust in a sheared-flow-stabilized Z pinch](#)

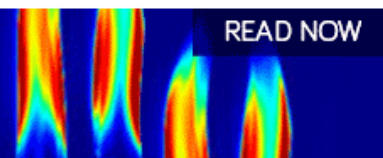
Physics of Plasmas **27**, 092510 (2020); <https://doi.org/10.1063/5.0018429>

### [Two-fluid and kinetic transport physics of Kelvin–Helmholtz instabilities in nonuniform low-beta plasmas](#)

Physics of Plasmas **27**, 102109 (2020); <https://doi.org/10.1063/5.0014489>

AIP Advances  
Fluids and Plasmas Collection

READ NOW



# Flow Z-pinch plasma production on the FuZE experiment

Cite as: Phys. Plasmas **27**, 112503 (2020); doi: 10.1063/5.0020481

Submitted: 1 July 2020 · Accepted: 24 September 2020 ·

Published Online: 3 November 2020



View Online



Export Citation



CrossMark

A. D. Stepanov,<sup>1,a),b)</sup> U. Shumlak,<sup>1,2</sup> H. S. McLean,<sup>3</sup> B. A. Nelson,<sup>2</sup> E. L. Claveau,<sup>1</sup> E. G. Forbes,<sup>1</sup> T. R. Weber,<sup>1</sup> and Y. Zhang<sup>2</sup>

## AFFILIATIONS

<sup>1</sup>Aerospace and Energetics Research Program, University of Washington, Seattle, Washington 98195, USA

<sup>2</sup>Zap Energy, Inc., Seattle, Washington 98104, USA

<sup>3</sup>Lawrence Livermore National Laboratory, Livermore, California 94550, USA

**Note:** This paper is part of the Special Collection: Papers from the 61st Annual Meeting of the APS Division of Plasma Physics.

**Note:** Paper N12 6, Bull. Am. Phys. Soc. **64** (2019).

<sup>a)</sup>Invited speaker.

<sup>b)</sup>Author to whom correspondence should be addressed: [astepano@uw.edu](mailto:astepano@uw.edu)

## ABSTRACT

The Fusion Z Pinch Experiment (FuZE) investigates sheared-flow stabilization of classic  $m = 0$  and  $m = 1$  instabilities in Z pinches with an embedded axial flow. FuZE consists of a 100 cm coaxial plasma accelerator, where neutral gas is ionized and accelerated in a pulsed electrical discharge, followed by a 50 cm assembly region, where pinches are formed. Maintaining the pinch requires continuous plasma injection provided by a deflagration mode in the coaxial accelerator. Two discharge modes, with and without deflagration, are investigated on FuZE. Pinch formation is observed with deflagration only. Plasma velocities in the assembly region are found to match the  $E \times B$  velocity estimated in the accelerator based on a 1D circuit model, indicating that a 1D MHD approximation may offer a valid description of the plasma in the accelerator channel. The velocity of magnetic field propagation is found to agree with the snowplow model based on momentum conservation, and the lifetime of the pinch is shown to be in agreement with constraints imposed by mass conservation.

Published under license by AIP Publishing. <https://doi.org/10.1063/5.0020481>

## I. INTRODUCTION

Recent years have seen increased interest in alternative low-cost approaches to thermonuclear fusion at intermediate densities of  $10^{18}$ – $10^{23}$  cm<sup>-3</sup>.<sup>1</sup> The Fusion Z pinch Experiment (FuZE)<sup>2,3</sup> at the University of Washington investigates a novel approach to Z pinches: sheared-flow stabilization. The Z pinch is a classic magnetic confinement concept<sup>4,5</sup> where an axial current in a cylindrical plasma column produces an inward  $j \times B$  force that compresses the plasma or maintains it in radial equilibrium against thermal expansion.<sup>6</sup> Early magnetic fusion research<sup>7–9</sup> found that Z pinches were catastrophically unstable to  $m = 0$  “sausage” and  $m = 1$  “kink” MHD modes, where  $m$  is the azimuthal mode number. These instabilities caused rapid loss of plasma confinement, severely hindering prospects for satisfying the Lawson criterion for thermonuclear energy gain.<sup>10</sup> If these instabilities can be suppressed, however, Z pinches become highly attractive for thermonuclear fusion due to the lack of external magnetic field coils, simple linear geometry, and high  $\beta$ .<sup>11</sup>

It is well-understood that the  $m = 0$  sausage mode can be stabilized with a tailored radial pressure profile satisfying the Kadomtsev criterion.<sup>12</sup> With a tailored radial pressure profile providing  $m = 0$

stability, the  $m = 1$  kink mode can be suppressed via sheared-flow stabilization. Sheared-flow stabilization requires the presence of an embedded axial flow in the Z pinch with radial variation of the axial velocity  $v_z(r)$ . Linear MHD stability analysis<sup>13</sup> gives the necessary magnitude of shear required to stabilize the  $m = 1$  mode as

$$\frac{dv_z}{dr} \geq 0.1kv_a, \quad (1)$$

where  $k$  is the axial wavenumber and  $v_a$  is the nominal Alfvén speed defined by maximum magnetic field and plasma density in the Z pinch. The basic stabilization mechanism can be considered as a form of phase mixing, where radial variation of the plasma axial velocity results in the “smearing out” of coherent structures, impeding their growth. The stabilizing effect of velocity shear in Z pinches has been investigated (and confirmed) in fluid,<sup>14</sup> kinetic,<sup>15</sup> and gyrokinetic<sup>16</sup> simulations.

Experimental investigation of shear-flow-stabilized (SFS) Z pinches<sup>14,17,18</sup> began on the Zap experiment at the University of Washington. The basic experimental configuration consists of a coaxial plasma accelerator, where flowing plasma is generated, coupled to

an assembly region, where sheared-flow Z pinches are formed. Low magnetic mode fluctuations were observed on ZaP when velocity shear was present in agreement with sheared-flow stabilization theory.<sup>14,17,18</sup> The current FuZE experiment (Fig. 1) is similar to the ZaP device, but with a driving capacitor bank and gas injection system designed to achieve higher currents. Recently, sustained neutron production lasting 10  $\mu$ s was observed on FuZE when operating with hydrogen–deuterium mixtures.<sup>2</sup> Emission of D–D neutrons was coincident with peak pinch current, quiescence in magnetic mode data, and  $\approx 1$  keV ion temperatures measured with ion Doppler spectroscopy.

This article investigates the production of flowing plasma in the accelerator based on velocity measurements in the assembly region and a 1D model that predicts the  $E \times B$  and snowplow velocities of the plasma. Data from two distinct discharge modes are presented. The first mode involves initial breakdown and current sheet (CS) formation in the middle of the accelerator, which allows for backward expansion of the conducting region in a deflagration mode associated with pinch formation.<sup>18</sup> We show that for the measured pinch current and flow velocity, the sheared-flow stabilization condition Eq. (1) can be readily satisfied, offering a plausible explanation for the 5  $\mu$ s persistence of the collimated pinch. The second mode is characterized by breakdown at the breech of the coaxial accelerator and the absence of deflagration. A series of spectroscopic measurements mapping the flow velocity in the assembly region were carried out for this mode. For both discharge modes, the  $E \times B$  velocity in the accelerator was in good agreement with velocities observed in the assembly region, indicating that a 1D MHD approximation may be applicable to the plasma in the coaxial accelerator.

The organization of this paper is as follows. Section II describes the experimental setup, details of the FuZE discharge, and diagnostics. Section III presents the experimental results for the discharge modes with and without deflagration. Discussion follows in Sec. IV, where methods for calculating the  $E \times B$  velocity and the snowplow model are presented and applied to experimental data, as well as estimates of the feasibility of sheared-flow stabilization and potential pinch lifetimes. Conclusions are given in Sec. V.

## II. EXPERIMENTAL APPARATUS AND METHODS

The FuZE device (Fig. 1) consists of a 100 cm coaxial accelerator coupled to a 50 cm assembly region. The inner and outer radii of the coaxial accelerator are 5 cm and 10 cm, respectively. The inner electrode is biased negatively while the outer electrode is grounded. Gas is introduced with fast-opening injection valves located in the middle of the coaxial accelerator. The capacitor bank has capacitance of 10 mF and series inductance of 0.2  $\mu$ H. Due to the large bank capacitance, the decrease in voltage on the bank capacitors is often negligible during a plasma pulse, with the bank effectively acting as a constant voltage source.

The evolution of the FuZE discharge is depicted in Fig. 2. After gas is injected at the midpoint of the coaxial accelerator, the capacitor bank is connected leading to breakdown in the middle of the accelerator where the neutral pressure is highest. A current sheet starts propagating in the direction of the  $j \times B$  force in a snowplow mode, ionizing and accelerating the neutral gas that it encounters. Once the plasma enters the assembly region, it converges radially, forming a pinch. To maintain the flow Z pinch, plasma must be continuously injected into the assembly region. On FuZE and its predecessor ZaP, continuous plasma supply occurs via a deflagration discharge mode in the accelerator. The deflagration mode in coaxial plasma accelerators<sup>18–22</sup> corresponds to the expansion of the current-carrying region in the opposite direction of the  $j \times B$  force. During deflagration, the neutral gas in the rear half of the accelerator is ionized and accelerated.

In the accelerator and the assembly region, the axial profile of the azimuthal magnetic field  $B_\phi(z, t)$  is measured with surface magnetic probes embedded in the inner surface of the outer electrode. The axial spacing between adjacent probes is 5 cm. Since the spatial derivative of  $B_\phi(z, t)$  is proportional to the radial current  $I_r$  at the outer electrode, the distribution of radial currents in the accelerator can be inferred from the magnetic probe data. The assembly region contains additional probes to measure the azimuthal dependence of the magnetic field  $B_\phi(z, \phi, t)$  at six axial locations ( $\Delta z = 10$  cm). Each axial location contains eight probes distributed uniformly along the azimuth. The probe signals are Fourier analyzed to determine the time evolution of

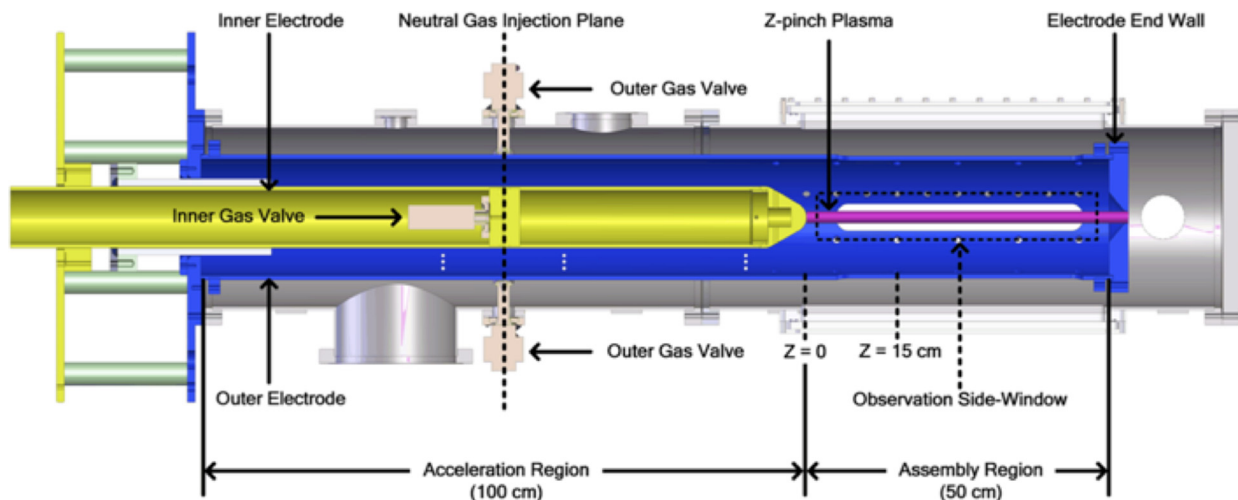


**FIG. 1.** Schematic of the FuZE device showing the 100 cm long coaxial accelerator coupled to a 50 cm long assembly region. An array of magnetic field probes measures the axial profile of the magnetic field  $B_\phi(z, t)$  with 5 cm axial resolution. Gas is injected in the middle of the accelerator from eight outer and one inner fast-opening injection valves.

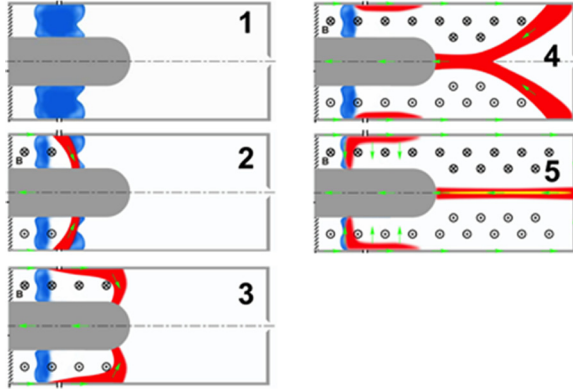


**FIG. 2.** Key stages of the FuZE discharge: (1) injection of neutral gas from fast-opening valves, (2) breakdown and propagation of the snowplow current sheet toward the assembly region, (3) plasma from the accelerator enters the assembly region, (4) a pinch is formed in the assembly region, and (5) accelerator continues to inject plasma into the assembly region, sustaining the pinch.

the amplitudes of the  $m = 1$  and  $m = 2$  azimuthal modes. These mode amplitudes are normalized by the average magnetic field at a given axial location (i.e.,  $m = 0$  mode amplitude). The quiescent period (QP) is defined when the normalized mode amplitude falls below a threshold of 0.2, which corresponds to a 1 cm radial displacement of the plasma column for the  $m = 1$  mode.<sup>23,24</sup> Because the start and end times of the QP vary somewhat between axial locations, an axial average of the normalized  $m = 1$  and  $m = 2$  mode amplitudes is used to determine the QP.

In the assembly region, optical access allows for spectroscopic measurements and direct imaging of the plasma with a Kirana fast camera at a 5 MHz frame rate. The ion Doppler spectroscopy diagnostic used to measure the axial plasma flow velocity images 10 chords through the plasma at a  $45^\circ$  angle to the flow with a telecentric viewing telescope.<sup>25</sup> The view chords are spaced 3.7 mm in the plasma, with 10 chords imaging a 3.3 cm wide span of the flow at one axial location. The plasma velocity is found from the Doppler shift of the carbon-III line at 229.7 nm and the carbon-V triplet at 227.1, 227.7, 227.8 nm. The light collected by each channel is chord-integrated through the plasma column. The bulk flow velocity which is calculated by averaging the velocity in each chord weighted by the brightness of the signal.

### III. RESULTS

#### A. Deflagration-sustained discharge

This section presents data for a typical deflagration-sustained discharge on FuZE. Pinch formation in the assembly region and its subsequent breakup were recorded with the Kirana fast camera. The discharge settings were as follows. The capacitor bank was charged to 5 kV, and the inner and outer gas injection valves, operating with 40 psia of hydrogen, were triggered at  $-1.20$  and  $-0.75$  ms, respectively. Figure 3 plots the current, voltage, and the averaged normalized mode data signals. The discharge voltage is measured at the breech of the accelerator ( $z = -100$  cm). We also plot the voltage at the nosecone ( $z = 0$ ). This signal is calculated by subtracting the inductive voltage drop along the accelerator from the measured voltage using Eq. (3) described later in Sec. IV. According to the mode data, the quiescent

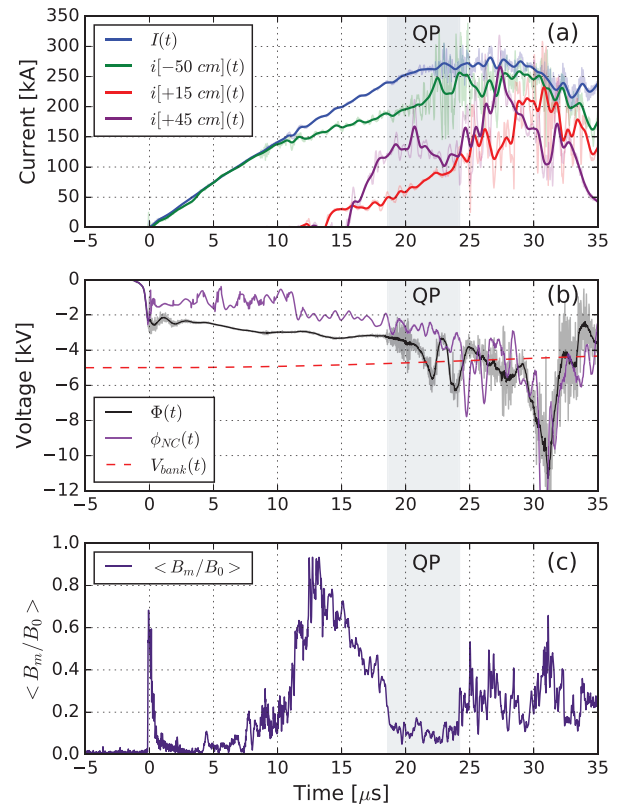


**FIG. 3.** (a) Total discharge current  $I(t)$  and currents in the middle of the accelerator ( $z = -50$  cm) and assembly region ( $z = 15$  cm and  $z = 45$  cm); (b) discharge voltage  $\Phi(t)$ , measured at  $z = -100$  cm, and the voltages calculated at the nosecone [Eq. (3)] and the capacitor bank; (c) average normalized mode data in the assembly region. The difference between  $I(t)$  and accelerator midplane current  $i(-50$  cm) corresponds to the current carried by the deflagration mode in the accelerator. Toward the end of the QP, the difference approaches zero, i.e., the deflagration current path terminates, resulting in a loss of plasma supply into the assembly region.

period (QP) occurs between  $19.6 \mu\text{s}$  and  $24.1 \mu\text{s}$ . During the QP, significant current (50–100 kA) is measured in the assembly region, while the amplitude of magnetic fluctuations is relatively low. These criteria provide a necessary condition for the presence of a shear-flow-stabilized Z pinch.

The azimuthal magnetic field profile measured by the probe array  $B_\phi(z, t)$  expressed as an axial current  $i(z, t) = 2\pi R_{\text{out}} B_\phi(z, t) / \mu_0$  is plotted in Fig. 4(a). The spatial derivative  $\partial i(z, t) / \partial z$ , which corresponds to the radial current per unit length in the accelerator, is plotted in Fig. 4(b). Three prominent current sheets (CSs) can be identified: snowplow, nosecone, and deflagration. The snowplow CS propagates forward from the location of initial breakdown in the middle of the accelerator ( $z = -50$  cm), reaching the assembly region ( $z = 0$ ) at  $t \approx 12 \mu\text{s}$ . Afterwards, a stationary CS is seen to form near the nosecone where the accelerator joins the assembly region. The deflagration current sheet initiates at  $z = -50$  cm at  $t \approx 12 \mu\text{s}$  and moves backwards, toward the breech of the accelerator, with a velocity of about 34 km/s. The deflagration CS terminates at  $t \approx 23.5 \mu\text{s}$ , upon reaching the breech of the accelerator. Within experimental



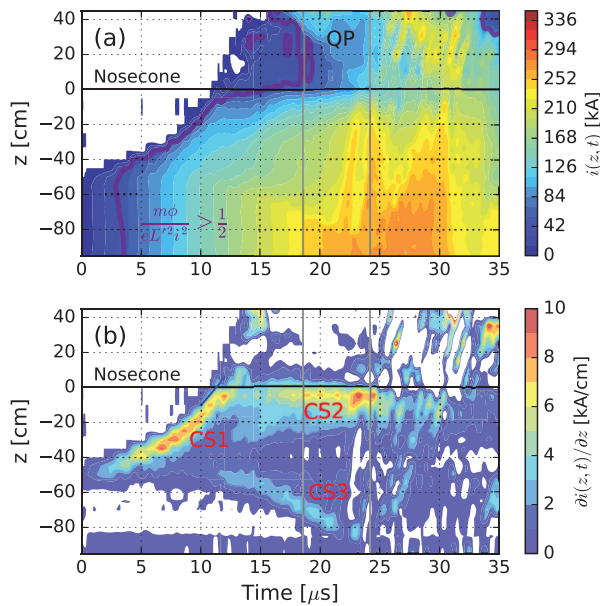


**FIG. 4.** (a) Azimuthal magnetic field profile measured by the probe array, expressed as an axial current  $i(z, t)$ ; (b) radial current in the accelerator. The radial current plot shows three prominent current sheets: the initial forward-moving snowplow (CS1), a stationary CS at the nosecone (CS2), and the backward-moving deflagration (CS3). The end of the QP is coincident with termination of deflagration when CS3 reaches the breach of the accelerator. A rapid forward propagation of the magnetic field in the accelerator is observed upon the shutoff of current conduction by CS3. The resulting inductive voltage spike can be seen in the voltage signal [Fig. 3(b)].

uncertainty, termination of deflagration is coincident with the end of the QP at  $t = 24.1 \mu\text{s}$ .

Frames from the Kirana fast camera are shown in Fig. 5 for a time interval that approximately coincides with the quiescent period, with the last three frames showing the initial stages of pinch breakup following the end of the QP. By tracking identifiable features in the video frames, such as a kink (F1) and the discontinuity in the axial structure of the pinch (F2/F3), the local flow velocities can be estimated as 123 km/s (F1) and 129 km/s (F2/F3). The earliest feature F1 has the appearance of a pure  $m=1$  kink mode, where a transverse displacement develops while axial uniformity is (approximately) maintained. In the later features (F1/F2), an axial discontinuity characteristic of a  $m=0$  sausage mode is observed in addition to the  $m=1$  transverse motion. Precise conclusions about the nature of these instabilities are hard to draw based on these images, however. The sensitivity of the Kirana camera is limited to the visible spectrum, while light emission from a hot pinch plasma is expected to be dominated by UV line radiation from highly stripped impurity ions (e.g., carbon-III and V). If the visible light observed by the camera is dominated by line radiation from periphery neutrals, its brightness should be proportional to the electron density at the edge of the pinch. Thus, the pinch would appear to have a greater radius than the actual radius of the hot plasma core.

## B. Discharge without deflagration

The second discharge mode without deflagration was encountered in an experimental campaign where the mass of the gas injected

into the accelerator was maximized in an attempt to reach higher currents. The injection valves were operated at a maximum plenum pressure of 300 psia with helium instead of hydrogen to further increase the injected mass. At high fill pressures breakdown occurred at the breach of the accelerator instead of the middle, leading to the absence of deflagration. The gas injection valves were triggered 1.8 ms before the initiation of the pulse, and the capacitor bank was charged to 7 kV.

Ion Doppler spectroscopy was used to measure the axial flow velocity of the plasma in the assembly region from carbon-III and carbon-V impurity lines. Only one velocity measurement could be obtained per plasma pulse at a single  $z$ -location in the assembly region. To measure the axial variation of the flow velocity and its time evolution, 24 pulses were acquired with  $1 \mu\text{s}$  exposures triggered between  $t = 36\text{--}60 \mu\text{s}$  at  $3 \mu\text{s}$  intervals and  $z = 10, 25$ , and  $40 \text{ cm}$ . Currents and voltage signals are shown in Fig. 6. The average of 24 pulses of the velocity survey is used to represent the data. The standard deviations of the signals over a set of 24 pulses provide the error bars in Fig. 6, demonstrating good shot-to-shot repeatability of the discharge. The peak discharge current was 650 kA, significantly higher than the current measured on pulses with lower injected mass. In the assembly region, currents of about 500 kA are measured. Due to deterioration of some of the magnetic probes in the assembly region, reliable azimuthal mode data could not be obtained, so the time interval of the quiescent period could not be determined.

The azimuthal magnetic field profile  $B_\phi(z, t)$  expressed as an axial current  $i(z, t)$  is plotted in Fig. 7. The current sheet distribution is distinctly different from the deflagration-sustained discharge described previously. Breakdown occurs near the breach ( $z = -95 \text{ cm}$ ) instead of the middle of the accelerator, with a single snowplow current sheet propagating toward the assembly region that reaches the nosecone at  $t = 32 \mu\text{s}$ . Afterwards, a stationary nosecone current sheet is established. No backward-moving deflagration current sheet is present in the data. Plasma velocities measured with ion Doppler spectroscopy in the assembly region are plotted over the magnetics data in Fig. 7. Initially, only carbon-III signal is observed with velocity of about 70 km/s. Carbon-V signal appears at  $t = 51 \mu\text{s}$  with a velocity of 240 km/s. Near the end wall, the velocity of the plasma is close to zero for both carbon-III and V signals, indicating plasma stagnation.

## IV. DISCUSSION

A flowing plasma is a key ingredient for sustaining the shear-flow-stabilized Z pinch configuration. The defining characteristic of a flow is velocity. Velocities between zero and 250 km/s are observed in the assembly region; these vary with time, spatial location, and impurity species sampled. The plasma observed in the assembly region is the product of a complex and dynamic discharge process taking place in the coaxial accelerator. Here, the lack of optical access limits available diagnostic to the magnetic probe array and the discharge voltage measured at the breach of the accelerator. This section begins by formulating methods to infer the flow velocity in the accelerator from these data based on the  $E \times B$  velocity and the snowplow model. We then consider the timing of plasma injection into the assembly region and the duration of the quiescent period, and show that basic considerations of mass conservation (accelerator cannot inject plasma indefinitely) can explain the duration of the quiescent period and pinch lifetime. We also address the plausibility of sheared-flow stabilization

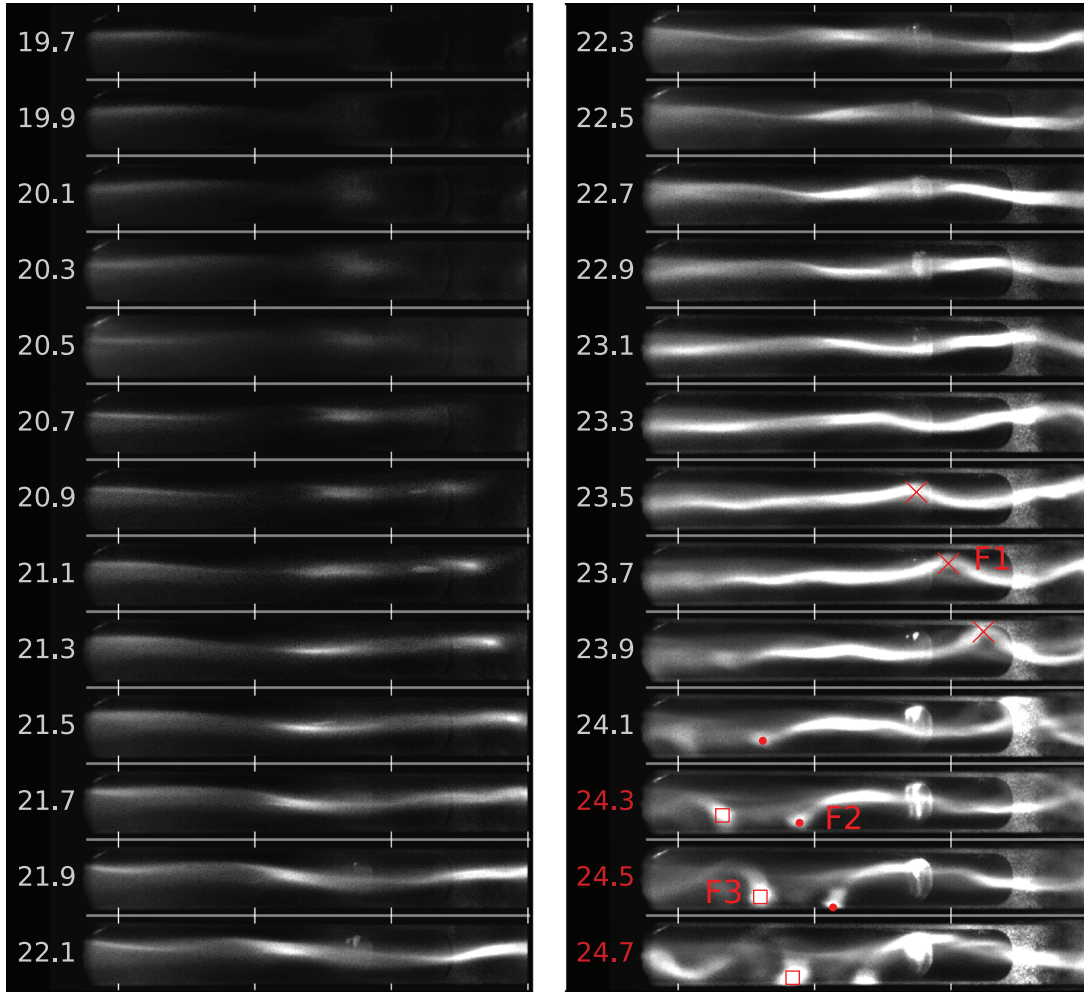


**FIG. 5.** Kirana frames of the assembly region (horizontal tick marks correspond to  $z = 15, 25, 35, 45$  cm). For each frame, the time in  $\mu\text{s}$  from the initiation of the pulse is indicated. All but the last three frames are taken during the quiescent period (19.6–24.1  $\mu\text{s}$ ). The final three frames demonstrate the start of the pinch breakup process after the end of the quiescent period. The velocity of the plasma can be estimated by tracking features in the flow. The earliest discernible feature (F1) occurs between  $t = 23.5$ – $23.9$   $\mu\text{s}$  and has a velocity of 123 km/s. Features F2 and F3, visible after the end of the QP, appear as a longitudinal disruption in the pinch structure in the vicinity of the nosecone moving with a velocity of 129 km/s.

in the pinch according to Eq. (1) by estimating the relative difference in velocity between the edge of the pinch and its center.

### A. $E \times B$ and snowplow velocity

The magnetic probe array on FuZE measures the axial distribution of the azimuthal magnetic field  $B_\phi(z, t)$  at the outer electrode that we express as an axial current  $i(z, t)$ . It is further useful to introduce the inductance per unit length parameter that characterizes the geometry of the coaxial accelerator

$$L' = \mu_0 \frac{\ln R_{\text{outer}}/R_{\text{inner}}}{2\pi} = 1.4 \times 10^{-7} \text{ H/m}.$$

Let  $\phi(z, t)$  be the distributed voltage on the inner electrode. Due to the inductive voltage drop generated by the time-varying axial current  $i(z, t)$ , the voltage  $\phi(z, t)$  satisfies

$$\frac{\partial}{\partial z} \phi(z, t) = -L' \frac{\partial}{\partial t} i(z, t). \quad (2)$$

Equation (2) is a well-known telegrapher's equation describing the spatial variation of the voltage along a lossless transmission line induced by a time-varying current  $i(z, t)$ . An additional assumption in Eq. (2) is that currents through the plasma between the inner and outer electrodes are purely radial, so  $B_\phi(r, z, t) = \mu_0 i(z, t)/2\pi r$ . The distributed voltage  $\phi(z, t)$  can be found by integrating Eq. (2) along  $z$  with the discharge voltage  $\Phi(t)$  measured at  $z_0 = -100$  cm as the boundary condition,

$$\phi(z, t) = \Phi(t) - L' \int_{z_0}^z \frac{\partial}{\partial t} i(z', t) dz'. \quad (3)$$

The second term on the RHS of Eq. (3) simply equals the rate of change of the magnetic flux between  $z_0$  and  $z$ . Note that since the total

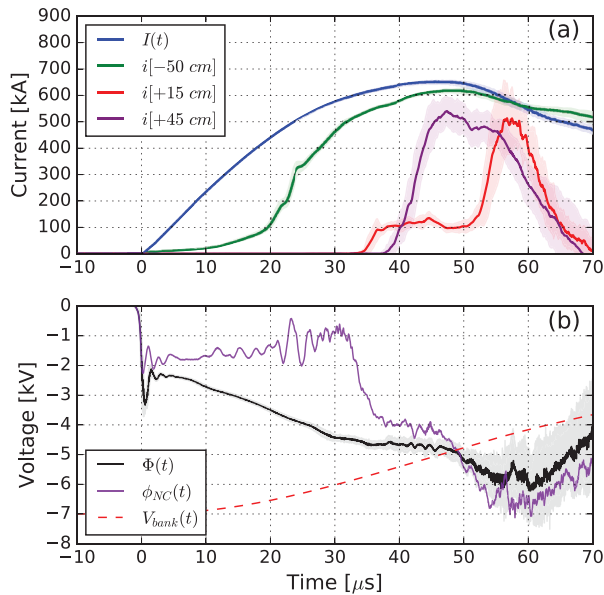


**FIG. 6.** Average (a) current and (b) voltage signals for 24 helium pulses. For each signal, the color shading indicates the standard deviation. The calculated nosecone voltage  $\phi_{NC}(t)$  and bank voltage  $V_{bank}(t)$  are plotted in (b). Currents of  $\sim 500$  kA are reached in the assembly region with high-pressure helium injection.

flux is known from the magnetic probe array, the time-varying inductance linked by the plasma can be found by dividing the flux by the discharge current.

From the current  $i(z, t)$  and voltage  $\phi(z, t)$  signals, one can estimate the local magnetic and electric field strengths in the accelerator.

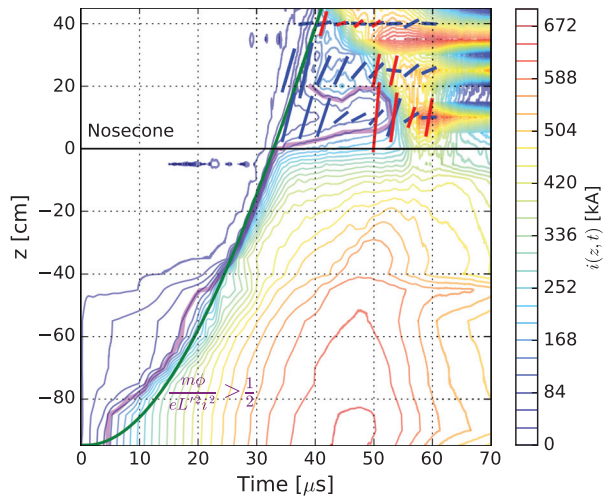


**FIG. 7.** Average magnetic field data for the 700 kA helium pulses. Carbon-III (blue dashes) and carbon-V (red dashes) velocities are plotted at the locations and times of the measurement. The snowplow trajectory  $z_{SP}(t)$  (green trace) is calculated from Eq. (10). The boundary of the  $E \times B$  condition of Eq. (7) is plotted in purple for helium. The initial carbon-III velocities appear to align with the magnetic field contours. Near-zero flow velocities near indicate plasma stagnation.

The relationship between the electric and magnetic fields and velocity is described by the generalized Ohm's law

$$\vec{E} + \vec{v} \times \vec{B} = \eta \vec{j}, \quad (4)$$

where  $\eta$  is the plasma resistivity and  $\vec{j}$  is the current density. The resistive term can be dropped for large values of the magnetic Reynolds number  $R_m = \mu_0 v l / \eta$ , where  $l$  is the length scale of the flow. Assuming Spitzer resistivity,  $R_m \approx 20$  for  $T_e = 1$  eV,  $l = 20$  cm, and  $v = 50$  km/s, i.e., ideal MHD is applicable so the plasma flow velocity should equal to the  $E \times B$  velocity.

Calculating the  $E \times B$  velocity from the current and voltage signals requires some caution. The radial distributions of the electric and magnetic fields, which determine  $v_{E \times B} = E(r)/B(r)$ , are not known *a priori*. In the absence of plasma, the electric field is purely radial  $E_r(r, z, t) = \phi(z, t)/(r \ln 2)$ . The magnetic field is purely azimuthal if there are no azimuthal currents ( $J_\phi = 0$ ), which we assume to be the case. If the currents through the plasma are purely radial ( $J_z = 0$ ), the magnetic field takes on the same form as the electric field:  $B_\phi(r, z, t) = \mu_0 i(z, t)/2\pi r$ . Since the electric and magnetic fields both vary as  $1/r$ , the amplitude of the  $z$ -directed  $E \times B$  velocity is independent of radius

$$v_{E \times B}(z, t) = \frac{E_r}{B_\phi} = \frac{1}{L'} \frac{\phi(z, t)}{i(z, t)}. \quad (5)$$

Thus, if the assumption that  $E, B \propto 1/r$  is satisfied, Eq. (5) unambiguously gives the bulk plasma flow velocity. Let us show that Eq. (5) retains some meaning for a general radial electric field distribution that can arise if sheaths develop in the plasma. Integrating the radial component of the generalized Ohm's law over radius replaces the unknown  $E_r(r)$  with the potential  $\phi$ , giving

$$\frac{1}{\ln 2} \int_{R_{in}}^{R_{out}} \frac{v_z(r) dr}{r} = \frac{1}{L'} \frac{\phi(z, t)}{i(z, t)}. \quad (6)$$

In this case, the  $E \times B$  velocity of Eq. (5) represents a particular integral moment of the actual flow velocity given by Eq. (6).

At high ion temperature, low density, and strong magnetic field, the ions become collisionless. For instance, collisionless conditions are reached at  $n_i = 10^{15} \text{ cm}^{-3}$ ,  $T_i = 50$  eV, and a current of 100 kA. In this case, for  $E \times B$  drift to be possible, the radial orbit excursion  $\approx v_{E \times B} / \Omega_c$  ( $\Omega_c$  is the cyclotron frequency) needs to be smaller than the 5 cm gap between the coaxial electrodes, so the particle does not collide with the channel walls. The necessary condition for passing ion orbits can be derived by considering the trajectory of an ion released from rest at the outer electrode. The ion will accelerate toward the cathode inner electrode by the applied electric field; for a passing orbit, the magnetic field has to be sufficiently strong to prevent the ion from striking the cathode. By integrating the equation of motion and invoking energy conservation, we can solve for the minimum radius attained by the ion to obtain the passing orbit condition ( $r_{min} > R_{in} = R_{out}/2$ )

$$\frac{m}{eL^2} \frac{\phi}{i^2} < \frac{1}{2}, \quad (7)$$

where  $m$  and  $e$  are particle mass and charge. For a typical discharge voltage of 1 kV, the minimum current required to satisfy Eq. (7) is 33 kA for protons.



The snowplow velocity  $v_{sp}$  is obtained from considerations of momentum conservation with the assumption that plasma acceleration is primarily due to  $j \times B$  forces. Then, the total axial force  $F(t)$  be found by integrating the magnetic pressure  $B^2/2\mu_0$  with the assumption that  $B \propto 1/r$ . The axial force,

$$F(t) = \int \frac{B^2}{2\mu_0} dA = \frac{1}{2} L' I(t)^2, \quad (8)$$

depends only on the discharge current and inductance per unit length  $L'$ .<sup>26</sup> Integrating  $F(t)$  in time gives the total impulse  $P(t)$ , which should equal the axial momentum of the plasma with mass  $M(t)$  and “snowplow velocity”  $v_{sp}(t)$ ,<sup>27</sup>

$$P(t) = M(t)v_{sp}(t) = \int_0^t F(t') dt' = \frac{L'}{2} \int_0^t I(t')^2 dt'. \quad (9)$$

The mass of the plasma is not directly measurable but is expected to increase in time as more of the neutral gas is ionized. A simple model of this process assumes a uniform linear mass density  $\lambda_0$  so  $M(t) = \lambda_0 z_{sp}(t)$  where  $z_{sp}$  is the distance traveled by snowplow. With the plasma momentum  $P(t) = \lambda_0 z_{sp}(t) v_{sp}(t) = d/dt (z_{sp}^2/2)$  known from Eq. (9), the following expressions for snowplow position and velocity can be obtained

$$z_{sp}^2(t) = \frac{2}{\lambda_0} \int_0^t P(t') dt', \quad (10)$$

$$v_{sp}(t) = \frac{P(t)}{\lambda_0 z_{sp}(t)}. \quad (11)$$

With fast gas injection employed on FuZE, the initial neutral fill profile will be non-uniform. In that case,  $\lambda_0$  can represent the average linear mass density in the accelerator, which can be approximated based on estimates of valve flow rates and injection timings.

## B. Interpretation of experimental data

The deflagration-sustained discharge described in Sec. III A can be considered a canonical example of FuZE operation, with breakdown occurring in the middle of the accelerator and subsequent formation of a backward-propagating deflagration current sheet. The images in Fig. 5 show pinch formation that begins with the start of the quiescent period and pinch breakup coincident with the termination of the QP. The visible discontinuity of the pinch near the nosecone (features F2 and F3 in Fig. 5) propagates at a velocity of 129 km/s. The velocity of the feature F1 observed a microsecond earlier near the end wall is approximately the same (124 km/s), so the flow velocity in the pinch is axially uniform near the end of the QP.

Let us estimate the amount of shear required to stabilize the pinch based on the stability condition of Eq. (1). We assume a linear mass density  $\lambda = 10^{-7}$  kg/m equal to the estimated initial fill density in the accelerator, and current  $I = 100$  kA that is known from the magnetic field measurements. Let  $\Delta v$  be the difference in velocity between the center and the edge of the pinch of radius  $R$ . With  $dv/dr = \Delta v/R$ , density  $\rho = \lambda/\pi R^2$ ,  $B = \mu_0 I/2\pi R$ , and  $k = 2\pi/R$ , Eq. (1) gives

$$|\Delta v| > 0.1 I \sqrt{\pi \mu_0 / \lambda} = 63 \text{ km/s}. \quad (12)$$

The velocity difference between pinch edge and center required for stabilization is smaller than the bulk flow velocity, so SFS is a

plausible mechanism responsible for the persistence of a collimated pinch for nearly 5  $\mu$ s. Regarding the cause for the termination of the QP, Eqs. (1) and (12) present three possibilities for violating the inequality: loss of shear, increase in current, or decrease in density. Of these, only the current is known based on diagnostic data. Figure 3 shows that in the course of the QP, the current at  $z = 15$  cm increases smoothly from 50 to 100 kA; it is possible, in principle, that the stabilization condition is violated due to the current exceeding a certain threshold. Another possibility is a decrease in density supplied from the accelerator. This hypothesis is perhaps consistent with the fact that deflagration terminates approximately 1  $\mu$ s before the end of the QP. In Fig. 3(a), the current in the middle of the accelerator ( $z = -50$  cm) is plotted. The difference between it and the total discharge current corresponds to the radial current conducted by the deflagration current sheet. This difference approaches zero at the end of the quiescent period.

Let us now consider possible explanations for the 4.5  $\mu$ s duration of the quiescent period. At a flow velocity of 125 km/s, the flow-through time for the 50 cm assembly region is 4  $\mu$ s, which is approximately equal to the QP duration. However, a causal link is not obvious here. Mass conservation may provide a better explanation for the duration of the QP. If the existence of a quiescent pinch requires plasma injection from the accelerator, then the duration of the QP must be limited by the available mass. If the linear mass density in the pinch approximately equals that in the accelerator, and only half of the mass initially present in the accelerator between the breech and the midpoint is supplied into the pinch by the deflagration wave, the estimated duration of plasma injection is again 4  $\mu$ s. Thus, the observed duration of the quiescent period is close to the expected duration of plasma injection.

The  $E \times B$  velocities calculated using Eq. (5) at the breech of the accelerator, midpoint, and nosecone are plotted in Fig. 8, as well as the velocities of the three features identified in the fast camera data. It is evident from Fig. 8 that the plasma velocity in the assembly region is close to the  $E \times B$  velocity inside the accelerator, but is significantly smaller, by a factor of 2, than the  $E \times B$  velocity near the nosecone.

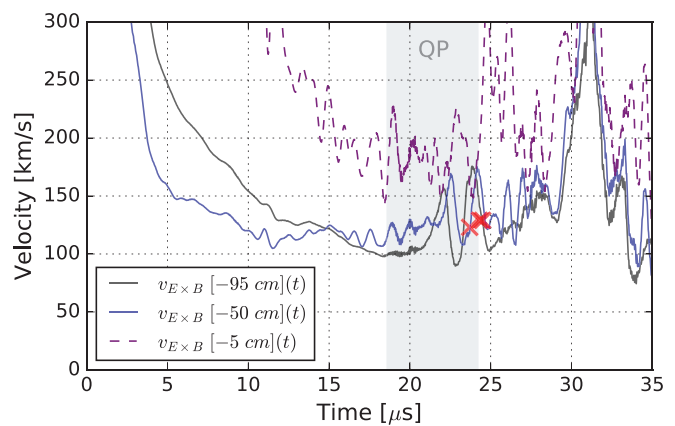


**FIG. 8.**  $E \times B$  velocity calculated in the accelerator at the breech, midpoint, and 5 cm upstream of the nosecone for the deflagration-sustained discharge. The velocity of features F1, F2, F3, indicated by the red crosses, is in good agreement with the  $E \times B$  velocity the accelerator but is substantially lower than  $v_{E \times B}$  predicted near the nosecone.



For the discharge mode without deflagration, the measured plasma velocities from carbon-III and carbon-V impurity lines are plotted over the magnetic field in the device in Fig. 7. Early in time ( $t < 40 \mu\text{s}$ ), only carbon-III lines are detected, consistent with the plasma having relatively low temperature. Carbon-III velocities closely match the slope of the magnetic field contours and the calculated snowplow trajectory plotted in the figure. Initial carbon-V emission is observed near the end wall at  $t = 42 \mu\text{s}$ , with a velocity of about 60 km/s. This observation of velocity by the end wall is an outlier in our data since no appreciable velocity is measured at later times, indicating plasma stagnation near the end wall. A local increase in magnetic field near the end wall is observed in the magnetic probe data. This effect may be due to compression of magnetic flux when moving magnetized plasma ejected from the accelerator collides with the stagnating plasma by the end wall. Carbon-V lines, indicative of hotter plasma, appear in the assembly region in the vicinity of the nosecone at  $t = 51 \mu\text{s}$ . The velocity of carbon-V is 214 km/s. At the same time, carbon-III velocity is only 20 km/s. A likely explanation for this difference is that the C-V signal is collected from the inner core of the pinch, where both temperature and velocity are higher compared to the edge. The edge plasma is, in turn, responsible for the C-III emission with a Doppler shift corresponding to a slower velocity.

The snowplow trajectory in Fig. 7 was calculated from Eq. (11) assuming a linear fill density of  $7 \times 10^{-6} \text{ kg/m}$ . This value was estimated from a known mass injection rate for the gas valves and the 1.8 ms duration of gas injection. The initial location of the snowplow was assumed to be near the breach of the accelerator, where breakdown took place. The snowplow model predicts the trajectory of the expanding magnetic field region remarkably well, and its velocity is in good agreement with the measured carbon-III plasma velocity. This agreement, however, becomes ever more striking if we recognize that the ideal snowplow model cannot be strictly valid here. The snowplow trajectory plotted in the figure is calculated under the assumption that all the mass assembles into a thin layer that moves with a velocity dictated by momentum conservation. In the snowplow model, all the available mass must assemble by the end wall at  $t \approx 42 \mu\text{s}$ . The continued injection of plasma from the accelerator into the assembly region, however, indicates that significant mass remains behind the snowplow. The interesting result here is that the magnetic field appears to follow the snowplow model while the average velocity of the plasma must be considerably slower.

The  $E \times B$  velocities in the accelerator and near the nosecone are plotted in Fig. 9 with the measured carbon-III/V plasma velocities and the snowplow velocity. Similar to what was observed in Fig. 8, there is agreement between the carbon-III velocity in the assembly region and the  $E \times B$  velocity in the middle of the accelerator, with the former only slightly exceeding the latter. When the carbon-V signal appears at  $t \approx 51 \mu\text{s}$ , its velocity (214 km/s) is significantly higher than the carbon-III flow velocity (60 km/s). Furthermore, the velocity of carbon-V is in good agreement with the  $E \times B$  velocity at  $z = +5 \text{ cm}$  near the nosecone.

The  $E \times B$  drift validity condition given by Eq. (7) lets us determine regions inside the accelerator where passing ion orbits are in principle possible. These regions are indicated in the contour plots of the magnetic field [Figs. 4(a) and 7]. We see that Eq. (7) is generally satisfied in the accelerator, but it may not be satisfied in the vicinity of the nosecone. In other words, the magnetic field at the nosecone is sufficiently low, and the voltage is sufficiently high

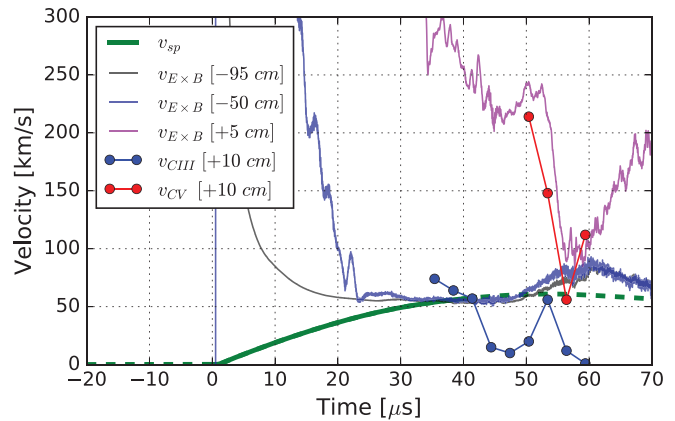


FIG. 9. Calculated  $E \times B$  velocities for the high pressure helium pulses compared to carbon-III/V plasma velocities measured in the assembly region at  $z = 10 \text{ cm}$  and the snowplow velocity. The  $E \times B$  velocities are shown for the accelerator breach, midpoint, and 5 cm downstream of the nosecone.

such that ions should be unable to pass from the accelerator into the assembly region without colliding with the inner electrode. It is interesting to note that in Fig. 4(a), the start of the quiescent period is coincident with the  $E \times B$  drift condition becoming satisfied everywhere in the assembly region. For the high pressure helium pulses (Fig. 7), a similar event is seen to occur at  $t \approx 53 \mu\text{s}$ , approximately coincident with the appearance of carbon-V emission near the nosecone.

## V. CONCLUSIONS

Sheared-flow-stabilized Z pinches require pulsed plasma flows with optimal parameters for pinch sustainment. Two distinct discharge modes were investigated on the FuZE device, distinguished by presence or absence of deflagration. With deflagration, a collimated pinch lasting  $5 \mu\text{s}$  was produced. The breakup of the pinch was coincident with termination of deflagration in the accelerator and the increase in magnetic fluctuations. The connection between the deflagration mode and pinch formation is also supported by the fact that for the discharge mode without deflagration, formation of a collimated pinch was not observed in the assembly region. With deflagration, the  $5 \mu\text{s}$  duration of the quiescent pinch was shown to be consistent the estimated possible duration of plasma injection from the accelerator. We also showed that for the density and velocity of the pinch, satisfaction of the sheared-flow stabilization condition is readily plausible. To analyze the operation of the coaxial accelerator, a 1D model was formulated for calculating the  $E \times B$  velocity of the flow from the experimental data. For both discharge modes, the velocities measured in the assembly region were in good agreement with the calculated  $E \times B$  velocities. The snowplow model was found to accurately predict the velocity of magnetic field propagation in the system. The 1D analysis presented in this article was able to explain the plasma flow velocities observed in the pinch and the duration of the quiescent period. With this foundation, future work will focus on developing 2D models to explain the formation of radial velocity shear required for pinch stabilization.

## ACKNOWLEDGMENTS

The information, data, or work presented herein was funded in part by the Advanced Research Projects Agency-Energy (ARPA-E), U.S. Department of Energy (DOE) under Award No. DE-AR-0000571, and the National Nuclear Security Administration under Grant No. DE-NA0001860.

## DATA AVAILABILITY

The data that support the findings of this study are available within the article.

## REFERENCES

- <sup>1</sup>C. L. Nehl, R. J. Umstadtd, W. R. Regan, S. C. Hsu, and P. B. McGrath, "Retrospective of the ARPA-E ALPHA fusion program," *J. Fusion Energy* **38**, 506–521 (2019).
- <sup>2</sup>Y. Zhang, U. Shumlak, B. A. Nelson, R. P. Golingo, T. R. Weber, A. D. Stepanov, E. L. Claveau, E. G. Forbes, Z. T. Draper, J. M. Mitrani, H. S. McLean, K. K. Tummel, D. P. Higginson, and C. M. Cooper, "Sustained neutron production from a sheared-flow stabilized Z-pinch," *Phys. Rev. Lett.* **122**, 135001 (2019).
- <sup>3</sup>U. Shumlak, "Z-pinch fusion," *J. Appl. Phys.* **127**, 200901 (2020).
- <sup>4</sup>W. H. Bennett, "Magnetically self-focusing streams," *Phys. Rev.* **45**, 890 (1934).
- <sup>5</sup>R. R. Spielman and J. De Groot, "Z pinches—A historical view," *Laser Part. Beams* **19**, 509 (2001).
- <sup>6</sup>M. G. Haines, "A review of the dense Z-pinch," *Plasma Phys. Controlled Fusion* **53**, 093001 (2011).
- <sup>7</sup>L. A. Artsimovich, A. M. Andrianov, O. A. Bazilevskaya, Y. G. Prokhorov, and N. V. Filippov, "An investigation of high-current pulsed discharges," *J. Nucl. Energy* **4**, 203 (1957).
- <sup>8</sup>A. S. Bishop, *Project Sherwood: The U.S. Program in Controlled Fusion* (Addison-Wesley Publishing Company, 1958).
- <sup>9</sup>W. A. Newcomb, "Hydromagnetic stability of a diffuse linear pinch," *Ann. Phys.* **10**, 232 (1960).
- <sup>10</sup>J. D. Lawson, "Some criteria for a power producing thermonuclear reactor," *Proc. Phys. Soc. B* **70**, 6 (1957).
- <sup>11</sup>U. Shumlak, B. A. Nelson, E. L. Claveau, E. G. Forbes, R. P. Golingo, M. C. Hughes, R. J. Oberto, M. P. Ross, and T. R. Weber, "Increasing plasma parameters using sheared flow stabilization of a Z-pinch," *Phys. Plasmas* **24**, 055702 (2017).
- <sup>12</sup>B. B. Kadomtsev, "Hydromagnetic stability of a plasma," *Rev. Plasma Phys.* **2**, 153 (1966).
- <sup>13</sup>U. Shumlak and C. Hartman, "Sheared flow stabilization of the  $m = 1$  kink mode in Z pinches," *Phys. Rev. Lett.* **75**, 3285 (1995).
- <sup>14</sup>U. Shumlak, B. A. Nelson, R. P. Golingo, S. L. Jackson, E. A. Crawford, and D. J. Den Hartog, "Sheared flow stabilization experiments in the ZaP flow Z pinch," *Phys. Plasmas* **10**, 1683 (2003).
- <sup>15</sup>K. Tummel, D. P. Higginson, A. J. Link, A. E. W. Schmidt, D. T. Offermann, D. R. Welch, R. E. Clark, U. Shumlak, B. A. Nelson, R. P. Golingo, and H. S. McLean, "Kinetic simulations of sheared flow stabilization in high-temperature Z-pinch plasmas," *Phys. Plasmas* **26**, 062506 (2019).
- <sup>16</sup>V. I. Geyko, M. Dorf, and J. R. Angus, "Gyrokinetic simulations of  $m = 0$  mode in sheared flow Z-pinch plasmas," *Phys. Plasmas* **26**, 062114 (2019).
- <sup>17</sup>U. Shumlak, R. P. Golingo, B. A. Nelson, and D. J. Den Hartog, "Evidence of stabilization in the Z-pinch," *Phys. Rev. Lett.* **87**, 205005 (2001).
- <sup>18</sup>R. P. Golingo, U. Shumlak, and B. A. Nelson, "Formation of a sheared flow Z-pinch," *Phys. Plasmas* **12**, 062505 (2005).
- <sup>19</sup>D. Y. Cheng, "Plasma deflagration and the properties of a coaxial plasma deflagration gun," *Nucl. Fusion* **10**, 305 (1970).
- <sup>20</sup>F. Poehlmann, N. Gascon, and M. Capelli, "The deflagration-detonation transition in gas-fed pulsed plasma accelerators," in *AIAA Joint Propulsion Conference* (2007), p. 5263.
- <sup>21</sup>K. T. K. Loebner, T. C. Underwood, and M. A. Cappelli, "Evidence of branching phenomena in current-driven ionization waves," *Phys. Rev. Lett.* **115**, 175001 (2015).
- <sup>22</sup>K. T. K. Loebner, T. C. Underwood, T. Mouratidis, and M. A. Cappelli, "Radial magnetic compression in the expelled jet of a plasma deflagration accelerator," *Appl. Phys. Lett.* **108**, 094104 (2016).
- <sup>23</sup>R. P. Golingo, "Modeling magnetic fields measured by surface probes embedded in a cylindrical flux conserver," *Rev. Sci. Instrum.* **78**, 033504 (2007).
- <sup>24</sup>U. Shumlak, C. Adams, J. Blakely, B. Chan, R. Golingo, S. Knecht, B. Nelson, R. Oberto, M. Sybouts, and G. Vogman, "Equilibrium, flow shear and stability measurements in the Z-pinch," *Nucl. Fusion* **49**, 075039 (2009).
- <sup>25</sup>D. J. D. Hartog and R. P. Golingo, "Telecentric viewing system for light collection from a Z-pinch plasma," *Rev. Sci. Instrum.* **72**, 2224 (2001).
- <sup>26</sup>R. G. Jahn, *Physics of Electric Propulsion* (McGraw-Hill, 1968).
- <sup>27</sup>M. Rosenbluth, R. Garwin, and A. Rosenbluth, "Infinite conductivity theory of the pinch," Technical Report No. LA-1850 (Los Alamos, 1954).